TRAIP promotes DNA damage response during genome replication and is mutated in primordial dwarfism

Margaret E. Harley[#1], Olga Murina[#1], Andrea Leitch[1], Martin R. Higgs[2], Louise S. Bicknell[1,17], Gökhan Yigit[3,4,5], Andrew N. Blackford[6], Anastasia Zlatanou[2], Karen J. Mackenzie[1], Kaalak Reddy[1], Mihail Halachev[1], Sarah McGlasson[1], Martin A. M. Reijns[1], Adeline Fluteau[1], Carol-Anne Martin[1], Simone Sabbioneda[7], Nursel H. Elcioglu[8], Janine Altmüller[3,9], Holger Thiele[9], Lynn Greenhalgh[10], Luciana Chessa[11], Mohamad Maghnie[12], Mahmoud Salim[8], Michael B. Bober[13], Peter Nürnberg[4,5,9], Stephen P. Jackson[6,14,15], Matthew E. Hurles[15], Bernd Wollnik[3,4,5,16], Grant S. Stewart[2], and Andrew P. Jackson[1]

[1]MRC Human Genetics Unit, IGMM, University of Edinburgh, Edinburgh, EH4 2XU, UK

[2]Institute of Cancer and Genomic Sciences, College of Medical and Dental Sciences, University of Birmingham, Birmingham, B15 2TT, UK

[3]Institute of Human Genetics, University Hospital Cologne, University of Cologne, 50931 Cologne, Germany

[4]Center for Molecular Medicine Cologne (CMMC), University of Cologne, 50931 Cologne, Germany

[5]Cologne Excellence Cluster on Cellular Stress Responses in Aging-Associated Diseases (CECAD), University of Cologne, 50931 Cologne, Germany

[6]The Gurdon Institute, University of Cambridge, Cambridge, CB2 1QN, UK

[7]Istituto di Genetica Molecolare, CNR, 27100 Pavia, Italy

[8]Department of Pediatric Genetics, Marmara University Pendik Hospital, Istanbul, Turkey

[9]Cologne Center for Genomics (CCG), University of Cologne, 50931 Cologne, Germany

[10]Cheshire and Merseyside Clinical Genetics Service, Liverpool Women's Hospital, Liverpool, L12 2AP, UK

[11]Department of Clinical and Molecular Medicine, University Sapienza, A.O.S. Andrea, I-00189 Roma, Italy

[12]Department of Pediatrics, IRCCS, Giannina Gaslini, University of Genova, 16147 Genova, Italy

Correspondence to APJ, andrew.jackson@igmm.ed.ac.uk, GSS, g.s.stewart@bham.ac.uk, or BW, bwollnik@uni-koeln.de.
[17]Present address: Department of Pathology, Dunedin School of Medicine, University of Otago, Dunedin, New Zealand

[13]Nemours/Alfred I. duPont Hospital for Children, Wilmington, Delaware 19803, USA

[14]Department of Biochemistry, University of Cambridge, Cambridge, CB2 1QN, UK

[15]Wellcome Trust Sanger Institute, Cambridge, CB10 1SA, UK

[16]Institute of Human Genetics, University Medical Centre Göttingen, 37073 Göttingen, Germany

[#] These authors contributed equally to this work.

Abstract

DNA lesions encountered by replicative polymerases threaten genome stability and cell cycle progression. Here we report the identification of mutations in *TRAIP*, encoding an E3 RING ubiquitin ligase, in patients with microcephalic primordial dwarfism/Seckel syndrome. We establish that TRAIP relocalizes to sites of DNA damage where it is required for optimal phosphorylation of H2AX and RPA2 during S-phase in response to UV irradiation, as well as fork progression through UV-induced DNA lesions. TRAIP is necessary for efficient cell cycle progression and mutations in TRAIP therefore limit cellular proliferation, providing a potential mechanism for microcephaly and dwarfism phenotypes. Human genetics thus identifies TRAIP as a novel component of the DNA damage response to replication-blocking DNA lesions.

INTRODUCTION

The rapid cellular response to genomic insults is facilitated by signaling cascades which utilize diverse post-translational modifications, particularly ubiquitylation and phosphorylation[1,2]. Mutations in genes encoding many components of DNA damage response (DDR) signaling pathways have been identified in human disease[1], reflecting the central importance of DNA repair in maintaining cellular homeostasis. Mutations in DDR genes have been associated with increased cancer predisposition, immunodeficiency, premature ageing and neurodegeneration[3,4]. Growth restriction and microcephaly are also features of certain DNA repair disorders[5-9]. Microcephalic primordial dwarfism (MPD) represents a group of single gene disorders[10] typically inherited as autosomal recessive traits, that includes Seckel syndrome[11,12], Microcephalic Osteodysplastic Primordial Dwarfism (MOPD) syndromes[13,14] and Meier-Gorlin syndrome[15,16]. In MPD, growth is restricted prenatally and remains severely restricted postnatally, resulting in an adult height as short as 1 meter[17]. Marked reduction in brain size, manifesting as microcephaly, distinguishes MPD from other forms of dwarfism, and mutations in genes encoding components of key cellular processes, including centrosome biogenesis, mitotic spindle function, replication licensing and DNA damage repair, have been identified in these disorders[10]. Particularly, multiple components of ATR-dependent DDR signaling have been implicated in Seckel syndrome and MOPD II, including mutations in *ATR*, *ATRIP*, *RBBP8* (encoding CtIP) and *PCNT*[7,8,18,19].

To identify further primordial dwarfism genes relevant to cell cycle and DNA repair processes, we performed whole-exome sequencing (WES) on a group of primordial dwarfism patients. Here, we report the identification of *TRAIP* as a novel human disease-

associated gene, and implicate the protein it encodes in regulating the DNA damage response to genotoxic lesions during replication.

RESULTS

TRAIP is a novel gene mutated in primordial dwarfism

We performed WES to establish a molecular diagnosis for a child with severe microcephalic primordial dwarfism. After filtering to remove common variants (minor allele frequency (MAF) > 0.005), analysis under a recessive inheritance model identified a homozygous nonsense mutation in *TRAIP*, c.553C>T, resulting in a premature stop codon, p.Arg185* (Fig. 1a). Sanger sequencing confirmed the presence of this mutation and its appropriate segregation in the family, with both parents being heterozygous carriers. The variant was not detected on sequencing of 380 control chromosomes, nor was it present in 1000 Genomes, EVS or EXaC public variant databases, in keeping with it being a rare recessive pathogenic mutation. Sanger resequencing of the coding exons and splice junctions of *TRAIP* in 262 primary microcephaly and primordial dwarfism patients identified a second patient, homozygous for the same mutation, p.Arg185*. Notably the two patients were born to non-consanguineous parents and originated from different countries with the families having no known relationship. However, high density genome-wide SNP genotyping demonstrated regions of homozygosity surrounding TRAIP in both patients of 4.6 and 8.4Mb respectively, consistent with unrecognized parental relatedness in each family (Supplementary Fig. 1a). As well, analysis of genome-wide SNP genotype data using FEstim[20] provided an inbreeding coefficient estimate of 0.003 for P2, equivalent to the inbreeding coefficient of 3rd cousin parents and also consistent with unknown parental consanguinity in this family (Supplementary Fig. 1b). Furthermore a 4.3 Mb homozygous haplotype was shared between P1 and P2 for the region immediately surrounding TRAIP, signifying a distant familial link with shared ancestry many generations previously despite their geographical separation (Supplementary Fig. 1a).

Additional WES on a cohort of patients with a presumptive diagnosis of Seckel syndrome (n=28), identified a further consanguineous family with a different mutation in *TRAIP*. In this family, a homozygous missense mutation was identified, c.52C>T, resulting in an arginine to cysteine substitution at codon 18 (p.Arg18Cys) (Fig. 1a). This highly conserved residue (Fig. 1b) lies within a RING domain, with the mutation resulting in a large physiochemical change, predicted bioinformatically to be deleterious (Alamut, Interactive Biosoftware Inc). The addition of a further cysteine residue is thought likely to be structurally deleterious, given that RING domains are defined by a specific motif of cysteine and histidine residues that bind zinc divalent cations to establish their tertiary structure[21].

The clinical phenotype of all three patients was remarkably similar (Fig. 1, Table 1, Supplementary Note). They shared almost identical growth parameters, with global growth failure of prenatal onset and extreme disproportionate microcephaly (Fig. 1c, Table 1). Neuroimaging demonstrated reduced cerebral cortical size with simplified gyral folding (Fig. 1d). Craniofacial similarities included a narrow elongated face and micrognathia (Fig. 1e). Additionally, significant morbidity from infections was evident. Patient 1 (P1) and Patient 2 (P2) had frequent lower respiratory tract infections, with P1 dying of respiratory

failure aged 10 years as a result of chronic lung disease. Furthermore, P1 had two siblings who died in early infancy[22]. However, aside from P2 who had a persistent lymphopenia, there was no evidence of adaptive immune deficits on clinical investigation.

On the basis of the mutations identified and phenotypic similarities between patients, we concluded that *TRAIP* was a novel gene associated with primordial dwarfism. TRAIP (TNF receptor associated factor (TRAF)-interacting partner; TRIP; RNF206) is a RING domain-type E3 ubiquitin ligase[23] originally identified as a negative regulator of innate immune signaling[24]. As it ubiquitylates TBK1[25], a key transducer of Toll-receptors and RIG-I, this could explain the recurrent respiratory illnesses in the patients; however the mechanistic basis for the primordial dwarfism phenotype was less evident. Therefore we proceeded to investigate the functional basis for the growth-related phenotypes.

TRAIP protein levels are markedly depleted in patient cells

We obtained cell lines from all three patients and characterized these to confirm the deleterious effect of mutations on the TRAIP protein. The Arg185* mutation introduces a premature stop codon in exon 7 and would be expected to cause nonsense-mediated decay of the *TRAIP* transcript. RT-PCR was therefore performed on RNA extracted from patient cells to assess transcript levels. This demonstrated marked reduction in *TRAIP* mRNA both in the immortalized lymphoblastoid cell line from P1 and a primary fibroblast cell line from P2 (Fig. 2a). Notably, low levels of residual full-length mRNA as well as alternatively spliced transcripts were evident. Cloning and sequencing of these RT-PCR products demonstrated that the latter included transcripts that are predicted to produce in-frame deletions of the TRAIP protein of 37 or 99 amino acids (Fig. 2a).

Immunoblotting was next performed to establish the consequence of the mutation at the protein level. TRAIP protein levels were greatly reduced in both patient cell lines P1 and P2 carrying the Arg185* mutation (Fig. 2b). A TRAIP protein of comparable size (47 kDa) to wild-type TRAIP (53 kDa) was only detectable on prolonged immunoblot exposure (Supplementary Fig. 2) while a truncated protein isoform of 184 amino acids was not observed, despite the polyclonal antibody (raised against residues 1-270) being able to efficiently detect both *in vitro* synthesized truncated and full-length proteins (Supplementary Fig. 3). In conjunction with RT-PCR findings, detection of residual TRAIP protein expression suggests that the mutation is a severe hypomorph, likely compromising, but not completely abrogating TRAIP cellular function. Consistent with this, a knockout mouse model established that *Traip* is essential for early embryonic development, with embryonic lethality seen at gastrulation and a reduction in cell number and embryo growth occurring as early as E5.5[26].

The Arg18Cys mutation had no effect on transcript levels (Supplementary Fig. 4), but also resulted in marked reduction of TRAIP protein levels in primary fibroblasts derived from patient P3 (Fig. 2b), probably reflecting reduced protein stability resulting from the missense mutation. We therefore concluded that patient TRAIP mutations would likely lead to substantial impairment of its cellular E3 ligase activity through depletion of overall protein levels.

TRAIP localizes to sites of UV-induced DNA damage

Phenotypically, TRAIP patients were reminiscent of individuals with Seckel syndrome that have defects in ATR pathway signaling[7,8], particularly with their disproportionately reduced head size. We therefore postulated that TRAIP could be a DDR protein acting in this pathway. Consistent with this, live-imaging of GFP-TRAIP protein demonstrated rapid re-localization from a pan-nuclear distribution to sites of DNA damage after UV laser microirradiation, irrespective of addition of BrdU as a DNA damage sensitizer (Fig. 3a). Colocalization was observed both with γH2AX and RFP-PCNA (Fig. 3b). Proximity ligation assays (PLA) detected GFP-TRAIP in close proximity (<40 nm) to PCNA in undamaged cells, suggesting it can be present at replication foci in undamaged cells. This association was substantially enriched after UV-C irradiation (Fig. 3c, d, p< 0.001), consistent with TRAIP localizing with PCNA at sites of DNA damage. Relocalisation of TRAIP to sites of UV-induced DNA damage was confirmed using localized UV-C irradiation through 3 μm isopore membrane filters, after which GFP-TRAIP was detected in irradiated regions, along with multiple DNA damage repair markers, including γH2AX and RPA2 (Fig. 3e). Notably, TRAIP was a highly significant hit in a recently reported high-throughput mass spectroscopy screen for proteins recruited to replication blocking DNA lesions[27]. As well as re-localizing to DNA damage sites, we also noted that TRAIP protein levels were regulated by DNA damage, with proteasome-mediated degradation observed at later time points after UV treatment (Supplementary Fig. 5), similar to certain DDR proteins involved in repair of UV lesions[28].

TRAIP is required for RPA2 and H2AX phosphorylation in S-phase

To assess whether TRAIP was a novel component of ATR-dependent DDR signaling, siRNA-depleted HeLa cells were irradiated with 10 J/m^2 UV and a time course was performed to monitor activation of this signaling pathway. Unlike ATR/ATRIP deficient cells[7,8], ATR-mediated phosphorylation of the downstream kinase CHK1 was not impaired by TRAIP depletion (Fig. 4a). Additionally, phosphorylation of the ATR substrates NBS1, SMC1 and Ser33-RPA2, as well as the activation of ATM and DNA-PK were also unaffected by TRAIP knockdown (Fig. 4a, Supplementary Fig. 6a, b). However, a striking reduction in phosphorylation of Ser4/Ser8-RPA2 and H2AX was seen in HeLa cells after TRAIP siRNA and in patient fibroblasts (Fig. 4b-e). Complementation of TERT-immortalized P2 fibroblasts (P2^{TERT}) by retroviral transduction of wild-type TRAIP (P2$^{TERT+TRAIP}$) restored RPA2/H2AX phosphorylation to normal levels after UV-C irradiation in P2$^{TERT+TRAIP}$ cells, confirming that these phosphorylation defects were directly due to loss of TRAIP (Fig. 4f, Supplementary Fig. 6c). Overall, phosphorylation of other ATR, ATM and DNA-PK substrates was comparable between P2^{TERT} and P2$^{TERT+TRAIP}$ cells (Supplementary Fig. 6d). Given this and the normal level of DNA damage-induced phosphorylation of multiple downstream substrates of ATR in siTRAIP-depleted cells, along with a normal G2/M checkpoint in response to UV irradiation (Supplementary Fig. 6e), we concluded that TRAIP deficiency did not give rise to a general defect in ATR signaling, but rather compromised phosphorylation of RPA and H2AX following the induction of UV damage.

Since DNA damage response to UV lesions occurs throughout the cell cycle, we next investigated when TRAIP is required to promote RPA2 and H2AX phosphorylation. Using quantitative immunofluorescence, we found that Ser4/Ser8-RPA2 and H2AX phosphorylation induced by UV-C exposure was significantly reduced in EdU-labeled TRAIP patient P2[TERT] cells but not in EdU-negative cells, indicating that TRAIP is specifically required during S-phase for optimal DNA damage- dependent phosphorylation of these proteins (Fig. 4g, Supplementary Fig. 7). Given that pSer4/Ser8- RPA2 has been associated with the resection of DNA double strand breaks (DSBs), a process that may occur when replication forks encounter UV lesions during S-phase, we considered whether differences in DSBs in patient cells could account for the altered RPA2/H2AX phosphorylation. To assess this, we performed neutral comet assays, which demonstrated equal levels of DSBs in TRAIP patient and control primary fibroblast cell lines after UV-irradiation (Supplementary Fig. 8). This indicated that reduced RPA2/H2AX phosphorylation was not a consequence of altered frequency of DSB formation. We therefore concluded that TRAIP is required for optimal H2AX and RPA2 phosphorylation in response to UV-induced damage encountered in S-phase.

Loss of TRAIP impairs cellular proliferation

We next considered how *TRAIP* mutations might reduce organism growth. Many primordial dwarfism genes are thought to cause reduced size through lowering the efficiency of cellular proliferation[10]. As TRAIP is required for efficient cell proliferation both in human primary cells and during mammalian development[26,29], we assessed the consequences of these mutations on growth rates of primary patient cell lines. We found that doubling times of patient fibroblasts (P2 and P3) were significantly slower than passage-matched control fibroblasts (Fig. 5a, c). Furthermore, this growth defect was complemented by retroviral transduction of patient cells with wild-type TRAIP (Fig. 5b), demonstrating that impaired proliferation was a direct consequence of TRAIP loss in patient cells, and indicating that prolonged cell cycle likely underlies the patient dwarfism phenotype.

To further characterize these cell cycle effects, we performed BrdU-pulse chase flow cytometry time courses using isogenic systems. Both TRAIP-depleted HeLa cells (Fig. 5d) and P2[TERT] patient cells (Supplementary Fig. 9b, c) retained higher 4n DNA content at later time points than matched controls (p = 0.0012, p=0.0135, respectively). This could not be accounted for by an increased percentage of mitotic cells (Supplementary Fig. 9a), and therefore represented an increase in late S-phase and/or G2 cells consistent with a replicative origin for the cell cycle delay.

To gain a further understanding of TRAIP's role during replication, we then examined replication fork dynamics in patient cells by DNA fiber analysis in patient cells. Replication fork velocity, inter-origin distance and fork stalling (1st label termination events) were not significantly altered in untreated TRAIP patient cells (Supplementary Fig. 10), suggesting that TRAIP deficiency does not result in significant global DNA replication defects. Given that TRAIP is required for efficient progression through S-phase and S-phase-specific alterations in RPA2/H2AX phosphorylation after DNA damage induction, we postulated that TRAIP is instead required when the replication fork encounters genotoxic lesions.

Consistent with this, following UV irradiation TRAIP patient cells exhibited significantly increased levels of fork stalling (Fig. 6a), and consequently substantially reduced levels of ongoing replicating forks. Moreover, while overall fork velocities were slowed in TRAIP patient cells after UV-C irradiation at rates comparable to control cells (Supplementary Fig. 11a), substantial fork asymmetry in TRAIP-deficient cells was observed (Fig. 6b, c), indicative of a problem with fork progression past bulky UV adducts. Importantly, P2[TERT+TRAIP] complemented cells exhibited normal levels of fork stalling (Supplementary Fig. 11b) and fork symmetry following UV-C irradiation (Supplementary Fig. 11c), establishing that TRAIP was specifically required to prevent fork stalling at UV lesions. Notably, levels of new origin firing were not increased in UV-C treated patient fibroblasts (Fig. 6a), indicating that the ATR-dependent intra-S-phase checkpoint remained intact. In contrast to UV, replication stress induced by low dose aphidicolin, or treatment with a cross-link inducing agent, mitomycin C (MMC), did not result in increased fork asymmetry in TRAIP patient cells compared with control cells (Supplementary Fig. 11c-e). Likewise, MMC treatment did not cause increased fork stalling in TRAIP-deficient cells (Supplementary Fig. 11c, d). Normal levels of fork recovery were also seen following replication fork stalling after hydroxyurea (HU) treatment (Supplementary Fig. 12), establishing that fork stability and replication restart are not generally impaired in TRAIP-deficient cells. Therefore, rather than a general requirement to promote genome replication under conditions of replication stress, TRAIP appears to have a role ensuring fork progression past bulky polymerase-stalling DNA lesions such as UV-photo-products.

DISCUSSION

Here, we report the identification of *TRAIP* as a human disease-associated gene and implicate it in DNA damage response to genotoxic lesions during genome replication. DNA damage encountered during S-phase is especially problematic, with substantial risks of mutation and/or genomic rearrangements arising from replication intermediates. Hence, multiple cellular mechanisms are employed to ensure replication fork stability and appropriate repair of DNA lesions[30]. Given our data demonstrating increased fork stalling and asymmetry following exposure to UV, but not HU, aphidicolin or MMC, TRAIP is likely to promote repair or bypass of replication blocking lesions induced by UV, rather than playing a general role in stabilizing or promoting restart of stalled replication forks.

A role for TRAIP in promoting translesion synthesis (TLS) has been raised by a developmental study of the Drosophila ortholog *nopo* which reported polyubiquitylation of DNA polymerase η (Pol η) [31]. However, the functional relevance of this observation is unclear since experiments were carried out in the absence of UV-induced damage. As well, Pol η undergoes active deubiquitylation in mammalian cells after UV irradiation to promote its recruitment to repair sites[32]. The patient phenotype is also inconsistent with a role for TRAIP in TLS, as it is distinct from Xeroderma-Pigmentosum-variant (XP-V)[33] that results from Pol η mutations[34,35]. XP-V manifests as freckling, increased sun sensitivity and skin cancer, rather than prenatal onset growth failure and microcephaly. TRAIP patients lack such dermatological features and cancer predisposition has not been observed, although all are still children. Furthermore, TRAIP cells do not exhibit the increased ATR pathway activation seen in XP-V cells[36]. Hence, TRAIP more likely acts in a parallel, TLS-independent

process, to overcome UV-C replication blocking lesions. TRAIP could instead be involved in a homologous recombination dependent mechanism to resolve such replication blocks, particularly given the role of RPA hyperphosphorylation in recruiting Rad51 after replication fork arrest[37]. Decreased RPA2 (and H2AX) phosphorylation might directly account for impaired fork progression at such UV-induced lesions, although how TRAIP promotes H2AX and RPA phosphorylation remains to be defined. TRAIP could act either by positively regulating a DDR protein kinase at UV-induced damage sites, or suppressing PP2A or PP4 protein phosphatases that dephosphorylate γH2AX and pSer4/Ser8-RPA2[38-41].

Ubiquitylation regulates many key DNA damage response processes[2], with several DDR-associated E3 ubiquitin ligases, including BRCA1[42,43], RNF168[44] and FANCL[45] implicated in human disease. The identification of additional TRAIP ubiquitylation substrates will be important to understand the disease process, and will likely provide further insights into its role at replication blocking lesions. It also remains to be formally established if its DNA repair/replication roles are dependent on a functional RING domain, as TRAIP could have E3 ligase-independent functions.

Total cell number is the predominant determinant of size in mammals[46]. Similarly, reduced cellularity from early development is believed to cause primordial dwarfism[10], with decrease in neuronal number generated during neurogenesis underlying the microcephaly. The DNA replication machinery is implicated in other forms of microcephalic dwarfism[47-49] and replication stress during embryonic development underlies Seckel syndrome due to *ATR* mutations[50]. Therefore, perturbed cell cycle progression as a consequence of replication blocking lesions could account for the microcephaly and dwarfism present in our TRAIP patients. For the cellular studies described here, UV-C irradiation was used to generate replication-blocking lesions. Most commonly these will be bulky cyclobutane pyrimidine dimers, which are unlikely to be encountered in the embryo. However during development, different replication blocking DNA lesions are present, with potential candidates being those arising from oxidative damage[51] or aldehydes[52]. Therefore endogenous DNA lesions may pose difficulties for TRAIP-deficient cells during development, and result in depleted overall cell numbers (Model, Supplementary Fig. 13) that underlies other microcephalic dwarfism disorders [48,50,53].

In summary, we identify *TRAIP* as a novel disease-associated gene, and through investigating the cellular basis of the human phenotype establish its involvement in DDR. TRAIP promotes H2AX and RPA2 phosphorylation following replication-associated DNA damage, and assists fork progression at UV-induced replication blocking lesions. Developmentally viable alleles identified through human genetics will facilitate future studies investigating its roles during embryogenesis, while identification of TRAIP substrates and mechanistic studies of its role in response to DNA lesions encountered during DNA synthesis, will provide further insight into the key cellular processes maintaining genome stability during replication.

ONLINE METHODS

Research subjects

Genomic DNA from the affected children and family members was extracted from peripheral blood using standard methods or saliva samples using Oragene collection kits according to the manufacturer's instructions. Informed consent was obtained from all participating families and the studies were approved by the ethics review boards, the Scottish Multicentre Research Ethics Committee (04:MRE00/19) and the Ethics Committee of the University Hospital Cologne, Germany. Parents provided written consent for the publication of photographs of the affected individuals.

Exome sequencing and haplotype analysis

Exome sequencing of genomic DNA and variant filtering was performed as described previously[54,55]. Cohort resequencing was performed by Sanger sequencing of PCR products representing all coding exons of TRAIP (primer sequences available on request), with variant calling using MutationSurveyor (SoftGenetics Inc). Haplotype analysis was undertaken by SNP genotyping both patients using Affymetrix CytoScan 750K arrays. Genotypes were generated using Affymetrix Genotyping Console software and examined manually.

Inbreeding coefficients for P1 and P2 were estimated using FEstim[20], using SNP genotypes with confidence scores $< 10^{-4}$, after linkage disequilibrium (LD) pruning using PLINK v1.90b3o (64-bit) [56]. Runs of homozygosity (ROH) were also used to calculate F_{ROH} using PLINK, as described previously[57,58]. In brief, SNPs were excluded with NoCall frequency above 3% across individuals or with a minor allele frequency (MAF) $< 5\%$. ROH were defined as runs of at least 50 consecutive homozygous SNPs spanning at least 1.5 Mb, with less than a 1 Mb gap between adjacent ROHs and a density of SNP coverage within the ROH of no more than 50 Kb/SNP, with at most one heterozygous SNP and five NoCalls allowed per window.

Cell culture

Lymphoblastoid cell lines (LCLs) were maintained in RPMI 1640 supplemented with 15% fetal bovine serum, L-glutamine and penicillin/streptomycin antibiotics in 5% CO_2 and normoxic conditions. Lymphoblastoid cell lines were generated in house from peripheral blood samples by EBV transformation using standard methods. Dermal primary fibroblasts were grown from skin punch biopsies in AmnioMax medium (Life Technologies) and then maintained in Dulbecco's MEM (modified Eagle's medium; DMEM) supplemented with 10% fetal bovine serum, 5% L-glutamine and 5% penicillin/streptomycin antibiotics in 5% CO_2 and hypoxic 3% O_2 conditions. Patient cell lines were validated using Sanger sequencing and immunoblotting. HeLa cells were maintained in DMEM supplemented with 10% fetal bovine serum, 5% L-glutamine and 5% penicillin/streptomycin antibiotics in 5% CO_2 and normoxic conditions. HeLa (ATCC), U2OS and MRC5 (GDSC, Sussex) cells were cultured in DMEM supplemented with 10% fetal bovine serum, 5% L-glutamine and 5% penicillin/streptomycin antibiotics.

Stable cell lines were generated by Flp recombinase-mediated integration using HeLa-Flp-In T-REx host cells (gift from Stephen Taylor, University of Manchester[42]) transfected with pcDNA5/FRT/TO-EGFP (vector only or EGFP-TRAIP) and pCAGGS-Flp.e (gift from Dirk-Jan Kleinjan, University of Edinburgh). Transfected cells were selected using 5 μg/ml blasticidin and 400 μg/ml hygromycin and the resulting colonies were then expanded for testing. Protein expression was induced with 1 μg/ml tetracycline treatment. HeLa cells expressing RFP-PCNA were a gift from Agata Lichawska and Jörg Mansfeld, Gurdon Institute. Primary fibroblasts derived from P2 were immortalized with hTERT retroviral supernatant with 4 μg/ml polybrene and infected with pMSCV-vector only or pMSCV-TRAIP. Selection was performed using 750 ng/ml puromycin and 500 μg/ml neomycin. Expression of the protein was verified by Western blot (Supplementary Fig. 6c). All cell lines were routinely tested for mycoplasma.

Cell treatments

Plasmids and siRNA oligos were transfected in Opti-MEM reduced serum media using Oligofectamine (Life Technologies) according to the manufacturer's guidelines. The siRNA oligonucleotide sequences are listed in Supplementary Table 1a. Where indicated, cells were treated with 10 μM MG132 (Cayman Chemicals), 10 or 15 J/m^2 UV-C, 2 mM hydroxyurea (Sigma-Aldrich), 0.5 μM aphidicolin (Sigma-Aldrich), 50 ng/ml mitomycin C (Sigma-Aldrich) or 2 mM thymidine (Sigma-Aldrich).

RT-PCR

Total RNA was extracted from cell lines using the RNeasy kit (Qiagen) according to the manufacturer's instructions. DNA was removed by treatment with DNase I (Qiagen) and cDNA was generated using random oligomer primers and AMV RT (Roche). The RT-PCR primer pairs used are listed in Supplementary Table 1b.

Western blot analysis and antibodies

Whole cell extracts were obtained by lysis and sonication of cells in UTB buffer (8 M Urea, 50 mM Tris pH 7.5, 150 mM β-mercaptoethanol, protease inhibitor cocktail (Roche)) or in NP-40 lysis buffer (50 mM Tris pH 8.0, 280 mM NaCl, 0.5% NP-40, 0.2 mM EDTA, 0.2 mM EGTA, 10% Glycerol, 1 mM DTT, protease inhibitor cocktail (Roche), 1 mM PMSF, phosphatase inhibitors (40 mM NaF, 1 mM sodium orthovanadate)) and analyzed by SDS-PAGE following standard procedures. Protein samples were run on 6-12% acrylamide SDS-PAGE or 4-12% NuPage mini-gels (Life Technologies) and transferred onto nitrocellulose membrane. Immunoblotting was performed using antibodies to RPA2 (Santa Cruz, sc-28709; 1:1000), pS4/S8-RPA2 (Bethyl Laboratories, A300-245A; 1:1000), pS33-RPA2 (Bethyl Laboratories, A300-246A; 1:1000), H2A (Millipore, 07-146; 1:5000), γH2AX (Millipore, 05-636; 1:1000), actin (Sigma-Aldrich, A2066; 1:5000), vinculin (Sigma-Aldrich, V9264; 1:1000), pS966-SMC1 (Bethyl Laboratories, A300-050A; 1:1000), SMC1 (Abcam, ab9262; 1:2000), pS343-NBS1 (Cell Signaling Technology, 3001; 1:500), NBS1 (Oncogene, PC269T; 1:500), pS345-CHK1 (Cell Signaling Technology, 2341; 1:500), CHK1 (Santa Cruz, sc-8408; 1:1000), pT68-CHK2 (Cell Signaling, 2661; 1:500) , CHK2 (Santa Cruz, sc-9064; 1:500), pS1981-ATM (Cell Signaling, 4526; 1:500), ATM (Abcam, ab31842; 1:1000), pS2056-DNA-PKcs (Abcam, ab18192; 1:400), DNA-PKcs (Abcam,

ab32566; 1:1000), pS824-KAP1 (Bethyl Laboratories, A300-767A; 1:5000), KAP1 (Bethyl Laboratories, A300-274A; 1:10000), CDK1 (Sigma-Aldrich, P7962; 1:1000), cyclin A (Santa Cruz, sc-751; 1:1000), cyclin B1 (Cell Signaling Technology, 4135; 1:1000), pS10-Histone H3 (Millipore, 06-570; 1:1000), Histone H3 (Millipore, 07-690; 1:10,000), FLAG (Agilent, clone M2; 1:1000).

TRAIP antibody was generated from recombinant TRAIP protein using pGEX-4T-2-TRIP-N (gift from Robert Geahlen, Purdue University, USA). Antibody was affinity purified from rabbit sera (Eurogentec) and specificity established using patient cell lysates and RNAi.

Laser line assay

Laser micro-irradiation and live cell imaging were performed as described previously in supplemental methods of ref[59]. Plasmids were transfected into U2OS cells using *Trans*IT-LT1 (Mirus Bio), according to the manufacturer's instructions. Images were acquired using an Olympus FluoView 1000 confocal microscope.

Immunofluorescence: GFP-TRAIP localisation

MRC5 fibroblasts were transfected with EGFP-TRAIP using Lipofectamine 2000 (Life Technologies) according to the manufacturer's instructions. The cells were trypsinised and seeded onto coverslips 6 hours post-transfection. The following day, the cells were washed once in warm PBS and treated with 2 mM hydroxyurea for 24 h or irradiated either at 25 J/m^2 for global UV-C irradiation (fluency rate 0.8 $J/m^2/s$) or at 120 J/m^2 for local UV-C irradiation through isopore membrane 3 μM filters (Millipore) and fixed 1 h or 1.5 h post UV-C, respectively. Immunofluorescence (IF) was performed as previously described[60] with minor modifications. Briefly, the cells were either pre-extracted in CSK100 buffer and then fixed in 4% paraformaldehyde for 15 min at room temperature or fixed first and then permeabilized in 0.5% Triton-X100 in PBS at room temperature for 15 min. Primary and secondary antibodies' incubations were performed in IF buffer (3% BSA in PBS) for 1 hour at room temperature. Primary antibodies: XPC (Santa Cruz, 1:100), PCNA (PC10, Santa Cruz, 1:400), γH2AX (Millipore, 1:500), RPA2 (Calbiochem, 1:200); secondary antibodies: Alexa Fluor-594 or Alexa Fluor-488 (Molecular Probes); DAPI 0.4 μg/ml (Vectashield). For EdU detection, cells were pulsed with 20 μM EdU for 20 min and then detected using the Click-iT EdU Imaging kit (Life Technologies) according to the manufacturer's protocol. Fluorescence images were taken using a Nikon E600 Eclipse microscope equipped with a 60X oil lens, and images were acquired and analysed using Volocity Software v4.1 (Improvision).

Proximity ligation assay (PLA)

Cells from stable EGFP/ EGFP-TRAIP HeLa Flp-In T-REx cell lines were fixed with methanol at −20 °C for 10 min followed by a 5 min extraction in 0.3% Triton-X100 in PBS. Cells were then incubated in anti-PCNA antibody (Santa Cruz, PC10; 1:500) and anti-GFP antibody (Abcam, ab6556; 1:500), and *in situ* proximity ligation was performed using a Duolink Detection Kit in combination with anti-Mouse PLUS and anti-Rabbit MINUS PLA Probes, according to the manufacturer's instructions (Sigma Aldrich Duolink). Nuclear foci were imaged using a Nikon E600 Eclipse microscope equipped with a 60X oil lens, and

images were acquired and analysed using Volocity Software v4.1 (Improvision). The number of nuclear foci/cell was quantified using ImageJ. More than 50 cells were analyzed per experiment per condition.

Quantitative immunofluorescence of pSer4/Ser8-RPA2 and γH2AX

Passage-matched TERT-immortalized fibroblasts were seeded on coverslips, 24 h later damaged with 15 J/m2 UV-C irradiation and left to recover for 4 hours in media containing 10 μM EdU. To remove soluble proteins prior to immunofluorescence, cells were pre-extracted for 10 min on ice with ice-cold buffer (25 mM Hepes 7.4, 50 mM NaCl, 1mM EDTA, 3 mM $MgCl_2$, 300 mM sucrose and 0.5% TritonX-100) and then fixed with 4% paraformaldehyde for 15 min. EdU immunolabeling was performed using Click-iT EdU Imaging Kit (Invitrogen, C10337) according to the manufacturer's protocol. Afterwards cells were stained for pS4/S8-RPA2 (Bethyl Laboratories, A300-245A; 1:1000) or γH2AX (Millipore, 05-636; 1:800) and then stained with secondary antibodies conjugated to Alexa Fluor-568 (Life Technologies) and DAPI. For quantification of signal integrated densities, images were visualized using a Zeiss Axioplan 2 microscope with iVision software (BioVision Technologies) and captured using 40X oil-immersion objective. Exposure time, binning, microscope settings and light source intensity were kept constant for all the samples. Nuclei were segmented on the basis of DAPI staining and then signal integrated density of pS4/S8-RPA2 and γH2AX staining quantified for each nuclear region using ImageJ software (US National Institutes of Health). More than 50 EdU positive and 150 EdU negative cells were analyzed per experiment per condition.

Comet assay

Neutral comet assays were carried out using the Trevigen Comet Assay™ electrophoresis kit (4250-050-K) according to manufacturer's instructions. Briefly, 1×10^5 primary fibroblasts were seeded in 6 well plates overnight for approximately 16 hours. Cells were then treated with 15 J/m^2 UV-C and allowed to recover for 4 hours in media. Cells were collected and embedded into low melting agarose on 'comet' slides (Trevigen) and incubated in lysis solution overnight in the dark at 4°C. Cells were then electrophoresed in buffer (50 mM Tris pH 9.0, 150 mM sodium acetate) for 45 min at 21 volts at 4°C in the dark. Comet slides were immersed in DNA precipitation solution (1 M ammonium acetate, 95% ethanol) for 30 min and 70% ethanol for 30 min at room temperature and dried at 37°C for 15 min. Slides were stained in 1x SYBR gold in TE buffer (pH 7.5) for 30 min at room temperature, dried for an additional 15 min at 37°C and then visualized with an epifluorescence microscope and analyzed using CaspLab software.

FACS analysis

Passage-matched TERT-immortalized fibroblasts grown in AmnioMax medium (Life Technologies) or HeLa cells were pulse labeled with 10 μM BrdU for 30 min before fixation with 70% ethanol at −20°C for 16 h. Cells were then digested with 1 mg/ml pepsin and denatured with 2 M HCl, before washing with PBS and blocking in 0.5% BSA, 0.5% Tween-20. BrdU labeling was detected using anti-BrdU antibody (Abcam, ab6326; 1:75) and FITC-conjugated anti-rat secondary antibody. DNA content was assessed by staining

with 50 μg/ml propidium iodide. Cells were sorted on a BD Biosciences FACS Aria II and data were analyzed using FlowJo software (v7.6.1, Tree Star).

Mitotic index of pulse labeled EdU cells

HeLa cells were seeded on poly-L-lysine-coated coverslips 48 h after siRNA transfection. The following day, 10 μM EdU was added to the cells for 30 min, washed out with PBS and media replaced. 6 h later cells were fixed using 4% paraformaldehyde and stained for pSer10-Histone H3 (Cell Signalling, 9706; 1:250) and EdU (Click-iT EdU Imaging Kit, Invitrogen, C10337) according to the manufacturer's protocol. Cells were then stained with secondary antibody conjugated to Alexa Fluor-568 (Life Technologies) and analyzed using a Zeiss Axioplan 2 microscope equipped with a 60X oil-immersion objectives and iVision software (BioVision Technologies).

G2/M checkpoint assay

A previously established assay was used to determine mitotic cell number after damage-induced checkpoint activation[61]. In brief, HeLa cells transfected with RNAi against TRAIP or luciferase (control) for 72 h were treated with 10 J/m^2 UV-C and fixed in 96% ethanol 4 h later. Mitotic cells were determined by pSer10-Histone H3 (Cell Signalling, 9706; 1:250) staining and flow cytometry on a BD Biosciences FACS Aria II.

DNA fiber spreading assay

Passage-matched primary or TERT-immortalized fibroblasts were pulse labeled with CldU for 20 min, washed with PBS and damaged with 30 J/m^2 UV-C, 2 mM hydroxyurea for 2 h or 0.5 μM aphidicolin before being pulse labeled with IdU for 20 or 40 min as indicated. 0.5 μM aphidicolin was added to the cells for 40 min together with IdU pulse labeling. 50 ng/ml mitomycin C was added to the cells for 24 h before CldU pulse labeling and left on during 20 min CldU and 20 min IdU pulse labeling. Cells were harvested by trypsinization and cell pellets were washed in PBS. 5×10^5 cells were lysed directly onto glass slides using spreading buffer (200 mM Tris-HCl pH 7.5, 50 mM EDTA, 0.5% SDS) and fixed in methanol:acetic acid (3:1 ratio). Following 2.5 M HCl denaturation, CldU was detected using rat anti-BrdU (clone BU1/75, ICR1; Abcam, ab6326; 1:750) and IdU was detected using mouse anti-BrdU (clone B44; BD Biosciences, 347583; 1:750). Slides were then fixed in 4% paraformaldehyde before immunostaining with secondary antibodies conjugated to Alexa Fluor-594 or Alexa Fluor-488 (Life Technologies). Labeled DNA fibers were visualized using a Zeiss Axioplan 2 microscope with iVision software (BioVision Technologies). Images were captured using 40X oil-immersion objectives and analyzed using ImageJ software (US National Institutes of Health).

In vitro transcription/translation

The TnT® T7 Quick Coupled Transcription/Translation System (Promega) was used to produce FLAG-tagged TRAIP (WT, R18C or R185X) *in vitro* following the manufacturer's instructions. Briefly, 250 ng of plasmid DNA (pcDNA-based, TRAIP with an N-terminal single FLAG epitope) in 2.25 μl of water was mixed with 10 μl TnT® T7 Quick Master Mix, 0.25 μl of 1 mM methionine and incubated for 90 min at 30°C. For immunoblotting 1

μl of each reaction was separated by SDS-PAGE on 4-12% NuPAGE gels (Life Technologies), and TRAIP was detected using anti-FLAG or anti-TRAIP antibodies.

Statistical analysis

Numerical data were analyzed using parametric and nonparametric statistical tests, namely Student's *t*-test, ANOVA or Mann Whitney Rank sum test, as indicated. Statistical tests were two-sided unless otherwise stated in figure legend. Significance thresholds are indicated in figure legends.

Supplementary Material

Refer to Web version on PubMed Central for supplementary material.

ACKNOWLEDGMENTS

AUTHOR CONTRIBUTIONS

M.E. Hurles, L.S.B., M. Halachev, G.Y., J.A., H.T., P.N., and B.W. performed exome sequencing and analysis. L.S.B., M.E. Harley, G.Y., S.M., and B.W. performed sequencing, genotyping, linkage analysis and other molecular genetics experiments. M.E. Harley, O.M., A.L., M.R.H., A.N.B., A.Z., K.R., M.A.M.R., A.F., C.-A.M., S.S., S.P.J. and G.S.S. designed and performed the cell biology experiments. N.H.E., L.G., L.C., M.M., M.S., M.B.B., K.J.M., and B.W. ascertained subjects, obtained samples and/or assisted with clinical studies. M.E. Harley and A.P.J. wrote the manuscript. The study was planned and supervised by B.W., G.S.S. and A.P.J.

REFERENCES

1. Ciccia A, Elledge SJ. The DNA damage response: making it safe to play with knives. Mol Cell. 2010; 40:179–204. [PubMed: 20965415]

2. Jackson SP, Durocher D. Regulation of DNA damage responses by ubiquitin and SUMO. Mol Cell. 2013; 49:795–807. [PubMed: 23416108]

3. Slatter MA, Gennery AR. Primary immunodeficiencies associated with DNA-repair disorders. Expert Rev Mol Med. 2010; 12:e9. [PubMed: 20298636]

4. Woods CG. DNA repair disorders. Arch Dis Child. 1998; 78:178–184. [PubMed: 9579166]

5. German J. Bloom's syndrome. I. Genetical and clinical observations in the first twenty-seven patients. Am J Hum Genet. 1969; 21:196–227. [PubMed: 5770175]

6. Murray JE, et al. Extreme growth failure is a common presentation of ligase IV deficiency. Hum Mutat. 2014; 35:76–85. [PubMed: 24123394]

7. O'Driscoll M, Ruiz-Perez VL, Woods CG, Jeggo PA, Goodship JA. A splicing mutation affecting expression of ataxia-telangiectasia and Rad3-related protein (ATR) results in Seckel syndrome. Nat Genet. 2003; 33:497–501. [PubMed: 12640452]

8. Ogi T, et al. Identification of the first ATRIP-deficient patient and novel mutations in ATR define a clinical spectrum for ATR-ATRIP Seckel Syndrome. PLoS Genet. 2012; 8:e1002945. [PubMed: 23144622]

9. Jackson SP, Bartek J. The DNA-damage response in human biology and disease. Nature. 2009; 461:1071–1078. [PubMed: 19847258]

10. Klingseisen A, Jackson AP. Mechanisms and pathways of growth failure in primordial dwarfism. Genes Dev. 2011; 25:2011–2024. [PubMed: 21979914]

11. Majewski F, Goecke T. Studies of microcephalic primordial dwarfism I: approach to a delineation of the Seckel syndrome. Am J Med Genet. 1982; 12:7–21. [PubMed: 7046443]

12. Seckel, HPG. Bird-Headed Dwarfs. S.Karger; Basel: 1960.

13. Majewski F, Ranke M, Schinzel A. Studies of microcephalic primordial dwarfism II: the osteodysplastic type II of primordial dwarfism. Am J Med Genet. 1982; 12:23–35. [PubMed: 7201238]

14. Majewski F, Stoeckenius M, Kemperdick H. Studies of microcephalic primordial dwarfism III: an intrauterine dwarf with platyspondyly and anomalies of pelvis and clavicles--osteodysplastic primordial dwarfism type III. Am J Med Genet. 1982; 12:37–42. [PubMed: 7201239]

15. Bongers EM, et al. Meier-Gorlin syndrome: report of eight additional cases and review. Am J Med Genet. 2001; 102:115–124. [PubMed: 11477602]

16. Gorlin RJ, Cervenka J, Moller K, Horrobin M, Witkop CJ Jr. Malformation syndromes. A selected miscellany. Birth Defects Orig Artic Ser. 1975; 11:39–50. [PubMed: 819054]

17. Rauch A, et al. Mutations in the Pericentrin (PCNT) Gene Cause Primordial Dwarfism. Science. 2008; 319:816–819. [PubMed: 18174396]

18. Griffith E, et al. Mutations in pericentrin cause Seckel syndrome with defective ATR-dependent DNA damage signaling. Nat Genet. 2008; 40:232–236. [PubMed: 18157127]

19. Qvist P, et al. CtIP Mutations Cause Seckel and Jawad Syndromes. PLoS Genet. 2011; 7:e1002310. [PubMed: 21998596]

20. Leutenegger AL, et al. Using genomic inbreeding coefficient estimates for homozygosity mapping of rare recessive traits: application to Taybi-Linder syndrome. Am J Hum Genet. 2006; 79:62–66. [PubMed: 16773566]

21. Borden KL, Freemont PS. The RING finger domain: a recent example of a sequence-structure family. Curr Opin Struct Biol. 1996; 6:395–401. [PubMed: 8804826]

22. Silengo M, Del Monaco A, Linari A, Lala R. Low birth-weight, microcephalic malformation syndrome in a 46,XX girl and her 46,XY sister with agonadism: third report of the Kennerknecht syndrome or autosomal recessive Seckel-like syndrome with previously undescribed genital anomalies. Am J Med Genet. 2001; 101:275–278. [PubMed: 11424145]

23. Besse A, Campos AD, Webster WK, Darnay BG. TRAF-interacting protein (TRIP) is a RING-dependent ubiquitin ligase. Biochem Biophys Res Commun. 2007; 359:660–664. [PubMed: 17544371]

24. Lee SY, Lee SY, Choi Y. TRAF-interacting protein (TRIP): a novel component of the tumor necrosis factor receptor (TNFR)- and CD30-TRAF signaling complexes that inhibits TRAF2-mediated NF-kappaB activation. J Exp Med. 1997; 185:1275–1285. [PubMed: 9104814]

25. Zhang M, et al. TRAF-interacting protein (TRIP) negatively regulates IFN-beta production and antiviral response by promoting proteasomal degradation of TANK-binding kinase 1. J Exp Med. 2012; 209:1703–1711. [PubMed: 22945920]

26. Park ES, et al. Early embryonic lethality caused by targeted disruption of the TRAF-interacting protein (TRIP) gene. Biochem Biophys Res Commun. 2007; 363:971–977. [PubMed: 17927961]

27. Raschle M, et al. DNA repair. Proteomics reveals dynamic assembly of repair complexes during bypass of DNA cross-links. Science. 2015; 348:1253671. [PubMed: 25931565]

28. Han C, et al. Cdt2-mediated XPG degradation promotes gap-filling DNA synthesis in nucleotide excision repair. Cell Cycle. 2015; 14:1103–1115. [PubMed: 25483071]

29. Almeida S, Ryser S, Obarzanek-Fojt M, Hohl D, Huber M. The TRAF-interacting protein (TRIP) is a regulator of keratinocyte proliferation. J Invest Dermatol. 2011; 131:349–357. [PubMed: 21068752]

30. Branzei D, Foiani M. Maintaining genome stability at the replication fork. Nat Rev Mol Cell Biol. 2010; 11:208–219. [PubMed: 20177396]

31. Wallace HA, et al. TRIP/NOPO E3 ubiquitin ligase promotes ubiquitylation of DNA polymerase eta. Development. 2014; 141:1332–1341. [PubMed: 24553286]

32. Bienko M, et al. Regulation of translesion synthesis DNA polymerase eta by monoubiquitination. Mol Cell. 2010; 37:396–407. [PubMed: 20159558]

33. Lehmann AR, McGibbon D, Stefanini M. Xeroderma pigmentosum. Orphanet J Rare Dis. 2011; 6:70. [PubMed: 22044607]

34. Masutani C, et al. The XPV (xeroderma pigmentosum variant) gene encodes human DNA polymerase eta. Nature. 1999; 399:700–704. [PubMed: 10385124]

35. Johnson RE, Kondratick CM, Prakash S, Prakash L. hRAD30 mutations in the variant form of xeroderma pigmentosum. Science. 1999; 285:263–265. [PubMed: 10398605]

36. Despras E, Daboussi F, Hyrien O, Marheineke K, Kannouche PL. ATR/Chk1 pathway is essential for resumption of DNA synthesis and cell survival in UV-irradiated XP variant cells. Hum Mol Genet. 2010; 19:1690–1701. [PubMed: 20123862]

37. Shi W, et al. The role of RPA2 phosphorylation in homologous recombination in response to replication arrest. Carcinogenesis. 2010; 31:994–1002. [PubMed: 20130019]

38. Nakada S, Chen GI, Gingras AC, Durocher D. PP4 is a gamma H2AX phosphatase required for recovery from the DNA damage checkpoint. EMBO Rep. 2008; 9:1019–1026. [PubMed: 18758438]

39. Chowdhury D, et al. A PP4-phosphatase complex dephosphorylates gamma-H2AX generated during DNA replication. Mol Cell. 2008; 31:33–46. [PubMed: 18614045]

40. Chowdhury D, et al. gamma-H2AX dephosphorylation by protein phosphatase 2A facilitates DNA double-strand break repair. Mol Cell. 2005; 20:801–809. [PubMed: 16310392]

41. Feng J, et al. Protein phosphatase 2A-dependent dephosphorylation of replication protein A is required for the repair of DNA breaks induced by replication stress. Mol Cell Biol. 2009; 29:5696–5709. [PubMed: 19704001]

42. Taylor SS, McKeon F. Kinetochore localization of murine Bub1 is required for normal mitotic timing and checkpoint response to spindle damage. Cell. 1997; 89:727–735. [PubMed: 9182760]

43. Soria G, Polo SE, Almouzni G. Prime, repair, restore: the active role of chromatin in the DNA damage response. Mol Cell. 2012; 46:722–734. [PubMed: 22749398]

44. Lancaster MA, Knoblich JA. Spindle orientation in mammalian cerebral cortical development. Curr Opin Neurobiol. 2012; 22:737–746. [PubMed: 22554882]

45. Lessel D, et al. Mutations in SPRTN cause early onset hepatocellular carcinoma, genomic instability and progeroid features. Nat Genet. 2014; 46:1239–1244. [PubMed: 25261934]

46. Conlon I, Raff M. Size control in animal development. Cell. 1999; 96:235–244. [PubMed: 9988218]

47. Bicknell LS, et al. Mutations in the pre-replication complex cause Meier-Gorlin syndrome. Nat Genet. 2011; 43:356–359. [PubMed: 21358632]

48. Bicknell LS, et al. Mutations in ORC1, encoding the largest subunit of the origin recognition complex, cause microcephalic primordial dwarfism resembling Meier-Gorlin syndrome. Nat Genet. 2011; 43:350–355. [PubMed: 21358633]

49. Guernsey DL, et al. Mutations in origin recognition complex gene ORC4 cause Meier-Gorlin syndrome. Nat Genet. 2011; 43:360–364. [PubMed: 21358631]

50. Murga M, et al. A mouse model of ATR-Seckel shows embryonic replicative stress and accelerated aging. Nat Genet. 2009; 41:891–898. [PubMed: 19620979]

51. Cooke MS, Evans MD, Dizdaroglu M, Lunec J. Oxidative DNA damage: mechanisms, mutation, and disease. FASEB J. 2003; 17:1195–1214. [PubMed: 12832285]

52. Langevin F, Crossan GP, Rosado IV, Arends MJ, Patel KJ. Fancd2 counteracts the toxic effects of naturally produced aldehydes in mice. Nature. 2011; 475:53–58. [PubMed: 21734703]

53. Frank KM, et al. DNA ligase IV deficiency in mice leads to defective neurogenesis and embryonic lethality via the p53 pathway. Mol Cell. 2000; 5:993–1002. [PubMed: 10911993]

METHODS-ONLY REFERENCES

54. Martin CA, et al. Mutations in PLK4, encoding a master regulator of centriole biogenesis, cause microcephaly, growth failure and retinopathy. Nat Genet. 2014; 46:1283–1292. [PubMed: 25344692]

55. Keupp K, et al. Mutations in WNT1 cause different forms of bone fragility. Am J Hum Genet. 2013; 92:565–574. [PubMed: 23499309]

56. Purcell S, et al. PLINK: a tool set for whole-genome association and population-based linkage analyses. Am J Hum Genet. 2007; 81:559–575. [PubMed: 17701901]

57. Joshi PK, et al. Directional dominance on stature and cognition in diverse human populations. Nature. 2015; 523:459–462. [PubMed: 26131930]

58. McQuillan R, et al. Runs of homozygosity in European populations. Am J Hum Genet. 2008; 83:359–372. [PubMed: 18760389]

59. Polo SE, et al. Regulation of DNA-end resection by hnRNPU-like proteins promotes DNA double-strand break signaling and repair. Mol Cell. 2012; 45:505–516. [PubMed: 22365830]

60. Despras E, Delrieu N, Garandeau C, Ahmed-Seghir S, Kannouche PL. Regulation of the specialized DNA polymerase eta: revisiting the biological relevance of its PCNA- and ubiquitin-binding motifs. Environ Mol Mutagen. 2012; 53:752–765. [PubMed: 23076824]

61. Stewart GS, Wang B, Bignell CR, Taylor AM, Elledge SJ. MDC1 is a mediator of the mammalian DNA damage checkpoint. Nature. 2003; 421:961–966. [PubMed: 12607005]
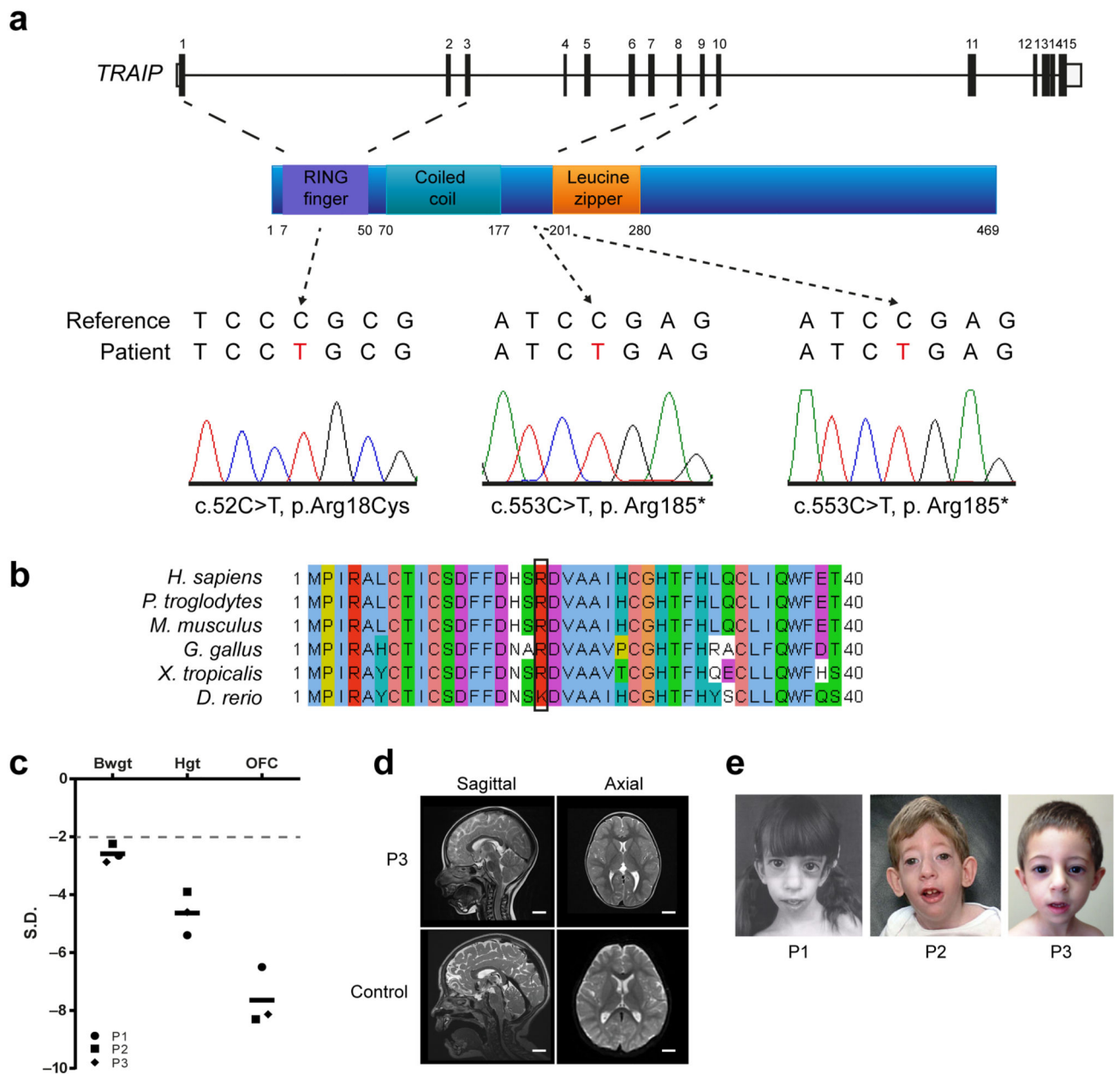
Figure 1. Mutations in *TRAIP* cause primordial dwarfism

(**a**) Mutations identified in *TRAIP*. Top, schematic of *TRAIP* gene structure; middle, TRAIP protein structure; bottom, sequence electropherograms demonstrating (middle, right panels) homozygous nonsense mutations in Patient 1 (P1) and Patient 2 (P2) and (left) a homozygous missense mutation, Arg18Cys in Patient 3 (P3). (**b**) A physiochemically similar residue is present at codon 18 in all vertebrates. Sequence alignments of *Homo sapiens, Pan troglodytes, Mus musculus, Gallus gallus, Xenopus tropicalis* and *Danio rerio* using Clustal W. (**c**) Patients with TRAIP mutations have prenatal onset severe growth failure with disproportionate microcephaly. Birth weight (BWGT), current height (HGT) and current head circumference (OFC) plotted as z-scores (standard deviations from population mean

for age and sex). 97.5% of general population will lie above the dashed line at −2 S.D. Black bars indicate mean values. (**d**) Cerebral cortical size is markedly reduced with simplification of gyral folding. MRI T2-weighted sagittal and axial images of P3 (age 3 years) compared with control scans of a healthy child (age 3 years 1 month). Scale bar, 2 cm. (**e**) Photographs of affected individuals with *TRAIP* mutations demonstrating facial similarities, including an elongated narrow face and micrognathia. Informed consent to publish photographs was obtained from families.
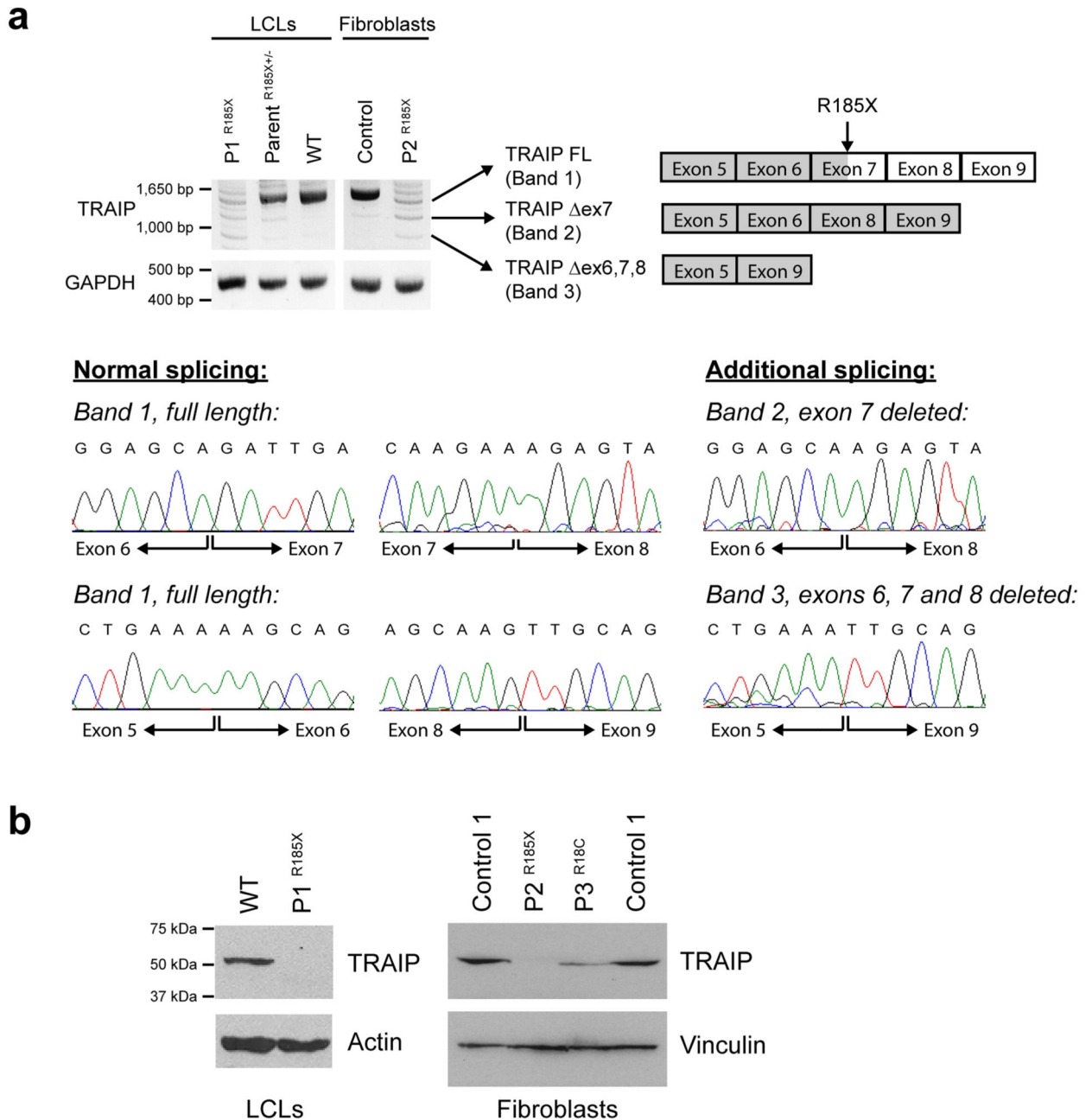
Figure 2. TRAIP mutations result in reduced cellular levels of TRAIP protein
(**a**) The Arg185* mutation severely reduces *TRAIP* transcript levels in P1 and P2 patient cell lines. RT-PCR using primers in 5′ and 3′ UTR to amplify *TRAIP* transcripts in primary fibroblasts and lymphoblastoid cell lines (LCLs) demonstrates marked decrease in full length *TRAIP* transcript, consistent with nonsense-mediated decay. Additional low intensity PCR products are evident, that represent alternatively spliced transcripts, confirmed by subcloning and Sanger sequencing (lower panels). These include transcripts, which through omission of exon 7, or exons 6, 7 and 8, retain an open reading frame and result in protein

products with small internal deletions. Loading control, *GAPDH*. (**b**) TRAIP protein levels are reduced in patients with Arg185* and the Arg18Cys mutations. Immunoblotting with an affinity purified rabbit anti-TRAIP antibody raised against recombinant TRAIP protein demonstrates reduced levels of the 53 kDa TRAIP protein in P3, and marked depletion in P1 and P2 where protein is only detectable on prolonged exposure (Supplementary Fig. 2). Loading controls, actin and vinculin.
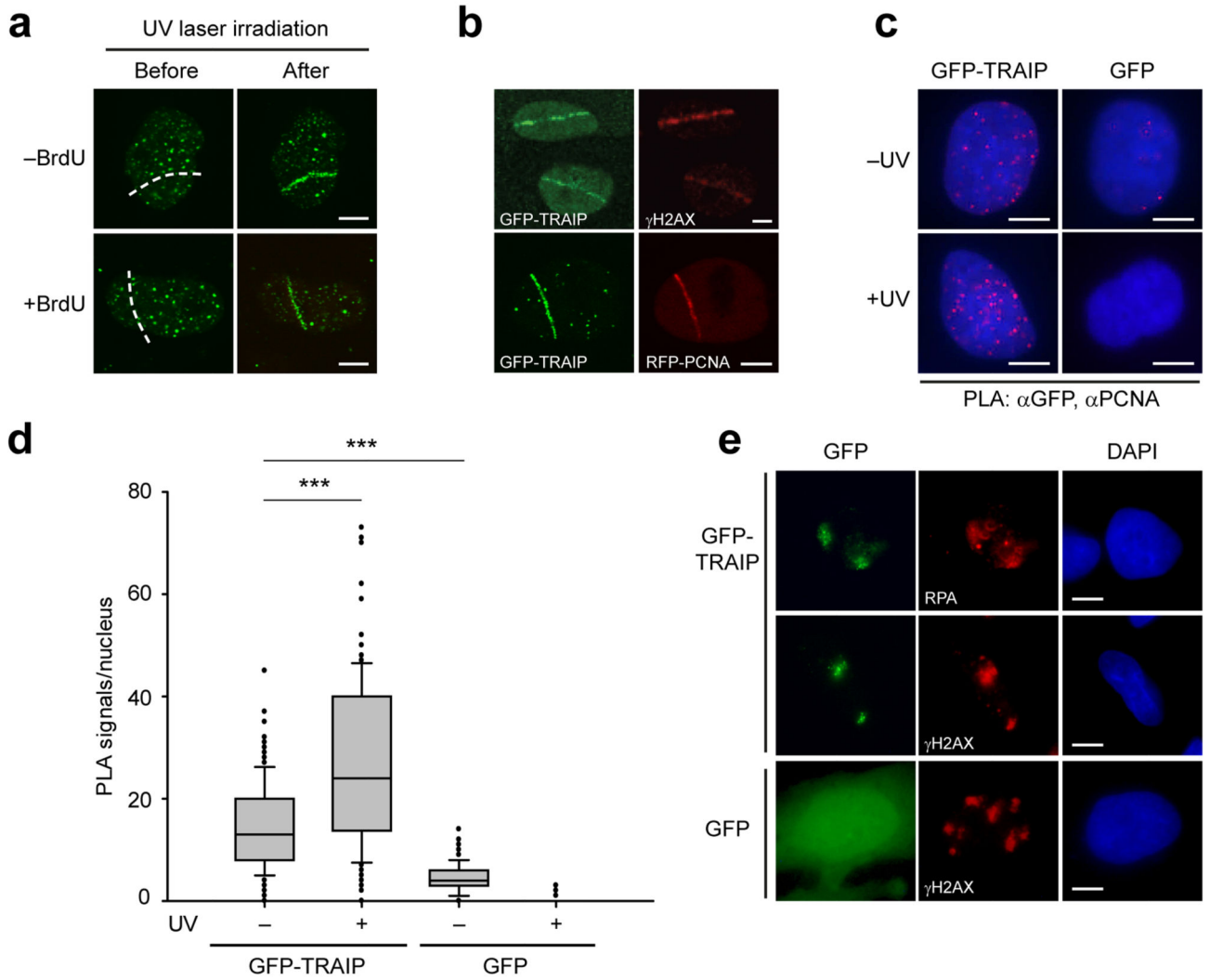
**Figure 3. TRAIP localizes to sites of UV-induced DNA damage**

(**a**) TRAIP localizes to DNA damage sites induced by UV laser microirradiation both in the absence and presence of pre-treatment with BrdU as a damage sensitizer. Representative images, before and after UV laser microirradiation. Scale bar, 5 μm. (**b**) GFP-TRAIP colocalizes with γH2AX and with RFP-PCNA at sites of UV laser-induced damage. Representative images of UV laser-irradiated GFP-TRAIP expressing cells immunostained for γH2AX (pre-sensitized with BrdU) or co-expressing RFP-PCNA (no BrdU pre-treatment) as indicated. Scale bar, 5 μm. (**c**, **d**) GFP-TRAIP is detected by a Proximity Ligation Assay (PLA) in close proximity to PCNA, an association enhanced after UV-induced damage. (**c**) Representative images of PLA signals/nucleus in doxycycline-inducible GFP-TRAIP HeLa cells before and after damage with 25 J/m^2 UV-C. Scale bar, 5 μm. (**d**) Quantification of PLA signals/nucleus. Box plots, center line denote mean values, box 25/75 %, whiskers 5/95 %, data pooled from n=2 independent experiments, n>65 data points per condition per experiment; Mann Whitney rank sum test: *** p<0.001. (**e**) TRAIP accumulates at sites of localized UV damage, colocalising with RPA and γH2AX.

Representative immunofluorescence images of MRC5 cells transfected with GFP-TRAIP or GFP alone after UV-C irradiation through 3 μm microfilters. Scale bar, 5 μm.
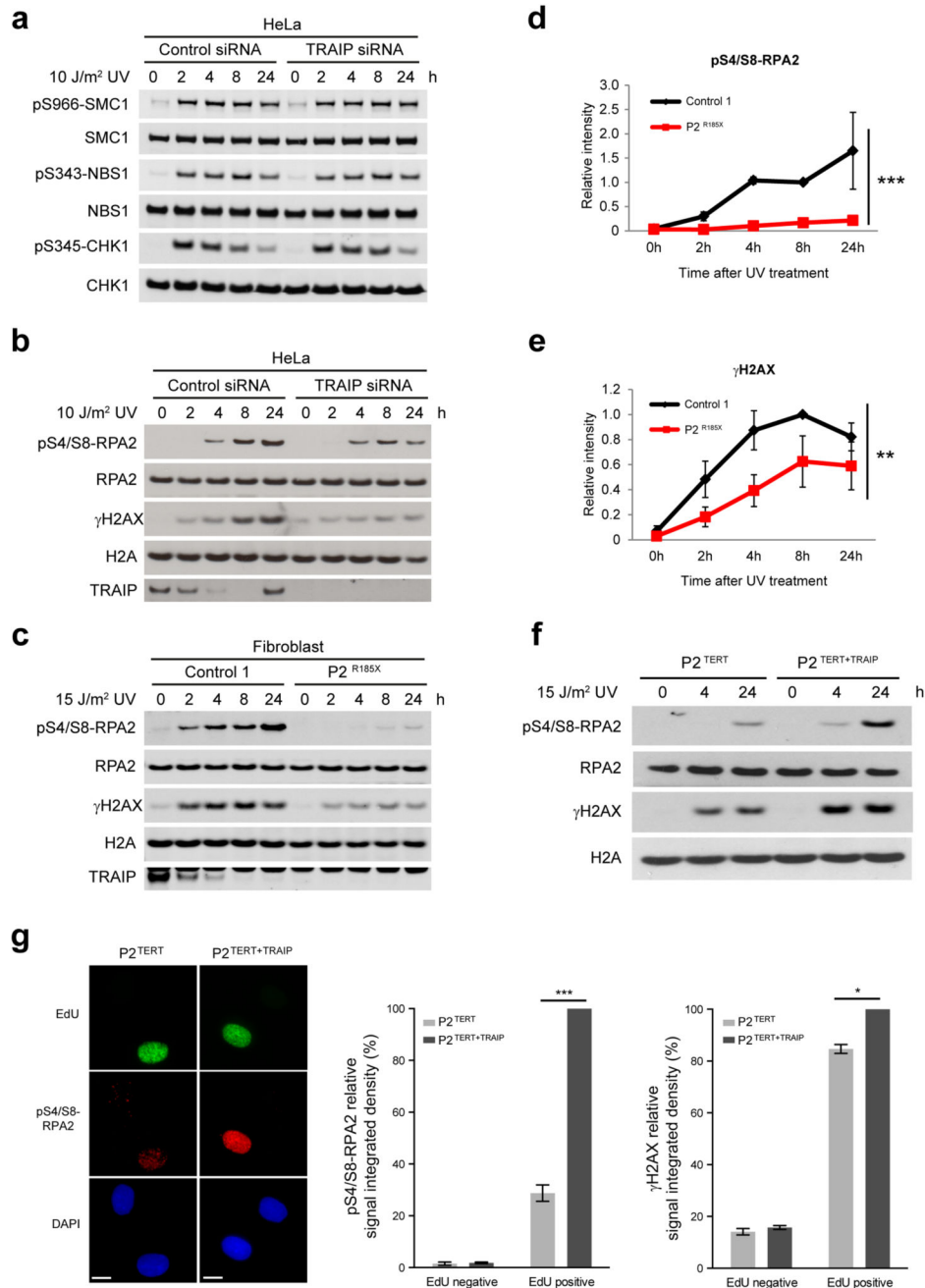
Figure 4. TRAIP is required for UV-induced RPA2 and H2AX phosphorylation during S-phase
(**a**) Phosphorylation of downstream ATR substrates is unaffected by TRAIP depletion. HeLa cells were transfected with RNAi against TRAIP or luciferase (control). After 72h, cells were UV-C treated, before harvesting at indicated times. Cell lysates were analyzed by Western blot as indicated. (**b**, **c**) TRAIP loss reduces RPA2 phosphorylation and histone H2AX phosphorylation (γH2AX) in response to UV. HeLa cells transfected with TRAIP and control siRNAs (**b**) or primary patient fibroblasts (**c**) were UV-C treated, harvested and immunoblotted as indicated. (**d**, **e**) Quantification of pS4/S8-RPA2 (**d**) and γH2AX (**e**) in

primary fibroblasts after UV. Chemiluminescence from Western blots quantified using ImageQuant. Mean ± SEM, n=3 experiments; values normalized to total RPA2 signal; two-way ANOVA across all time points: *** p<0.001, ** p<0.01. (**f**) Retroviral complementation with wild-type TRAIP rescues impaired phosphorylation of RPA2 and H2AX after UV-C irradiation in TRAIP^{Arg185*} cells. Fibroblasts derived from P2^{Arg185*} were immortalized with hTERT, denoted P2^{TERT}; and reconstituted with pMSCV-TRAIP, P2$^{TERT+TRAIP}$. (**g**) TRAIP is required for optimal RPA2 and H2AX phosphorylation in S-phase. P2^{TERT} and P2$^{TERT+TRAIP}$ cells were irradiated with 15 J/m^2 UV-C, labeled with EdU for 4 h, pre-extracted, fixed and co-stained for pS4/S8-RPA2 or γH2AX, EdU and DAPI. Representative images of immunofluorescence staining of pS4/S8-RPA2 (left), quantification of pS4/S8-RPA2 (middle) and γH2AX (right) signal integrated density in EdU-positive and EdU-negative cells. Mean ± SEM for n=3 experiments, values normalized to P2$^{TERT+TRAIP}$; Student's *t*-test: *p<0.05; ***p<0.001. Scale bar, 10 μm.
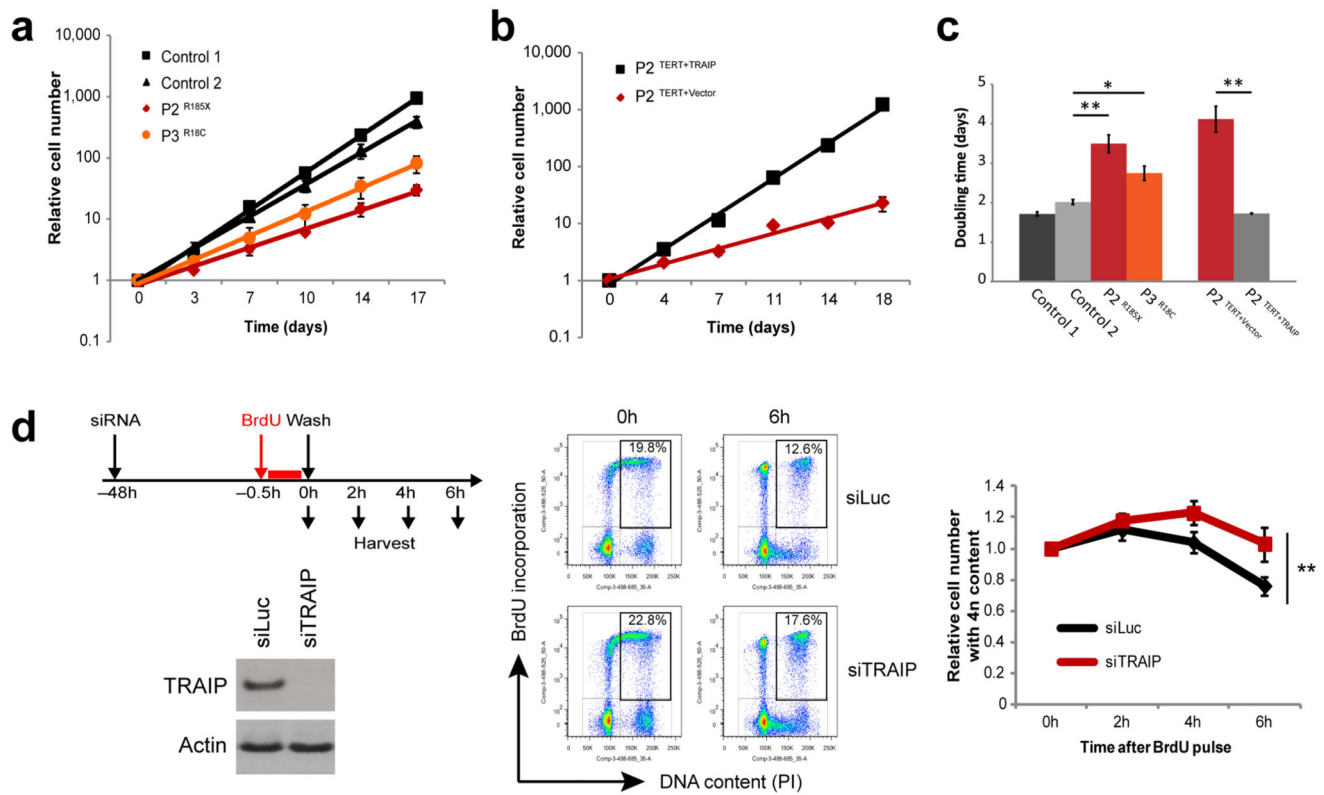
Figure 5. Impaired growth and cell cycle progression in TRAIP deficient cells
(**a**) TRAIP mutations impair cell proliferation. Cell numbers of passage-matched primary fibroblast cell lines derived from patients or controls were determined over 17 days to establish growth rates. Mean ± SEM for n=3 experiments; fold growth relative to day 0. (**b**) Complementation with wild-type TRAIP rescues the slow growth phenotype of TRAIP^{Arg185*} cells. P2^{TERT} fibroblasts were reconstituted with pMSCV-vector only or pMSCV-TRAIP. Growth rates of passage-matched cell lines were analyzed over 18 days. Mean ± SEM for n=3 experiments; fold growth relative to day 0. (**c**) Doubling times of fibroblast cells from (**a**) and (**b**). Mean ± SEM for n=3 experiments; Student's *t*-test: *p<0.05; **p<0.01. (**d**) TRAIP-depleted cells exhibit delayed S/G2 phase progression. HeLa cells were transfected with RNAi against TRAIP or luciferase (Luc) control. 72h later cells were pulse labeled with 10 μM BrdU for 30 min before washing out and replacing with fresh media. At indicated times, cells were harvested, fixed and prepared for flow cytometry. Left, Western blots of RNAi for TRAIP or control Luc demonstrate effective TRAIP depletion. Middle, representative images of gating used in analysis of flow cytometry data. Right, quantification of the relative number of cells with 4n content; fold change relative to 0h. Mean ± SEM, n=4 experiments. Fold change relative to 0h; two-way ANOVA across all time points: ** p<0.01.
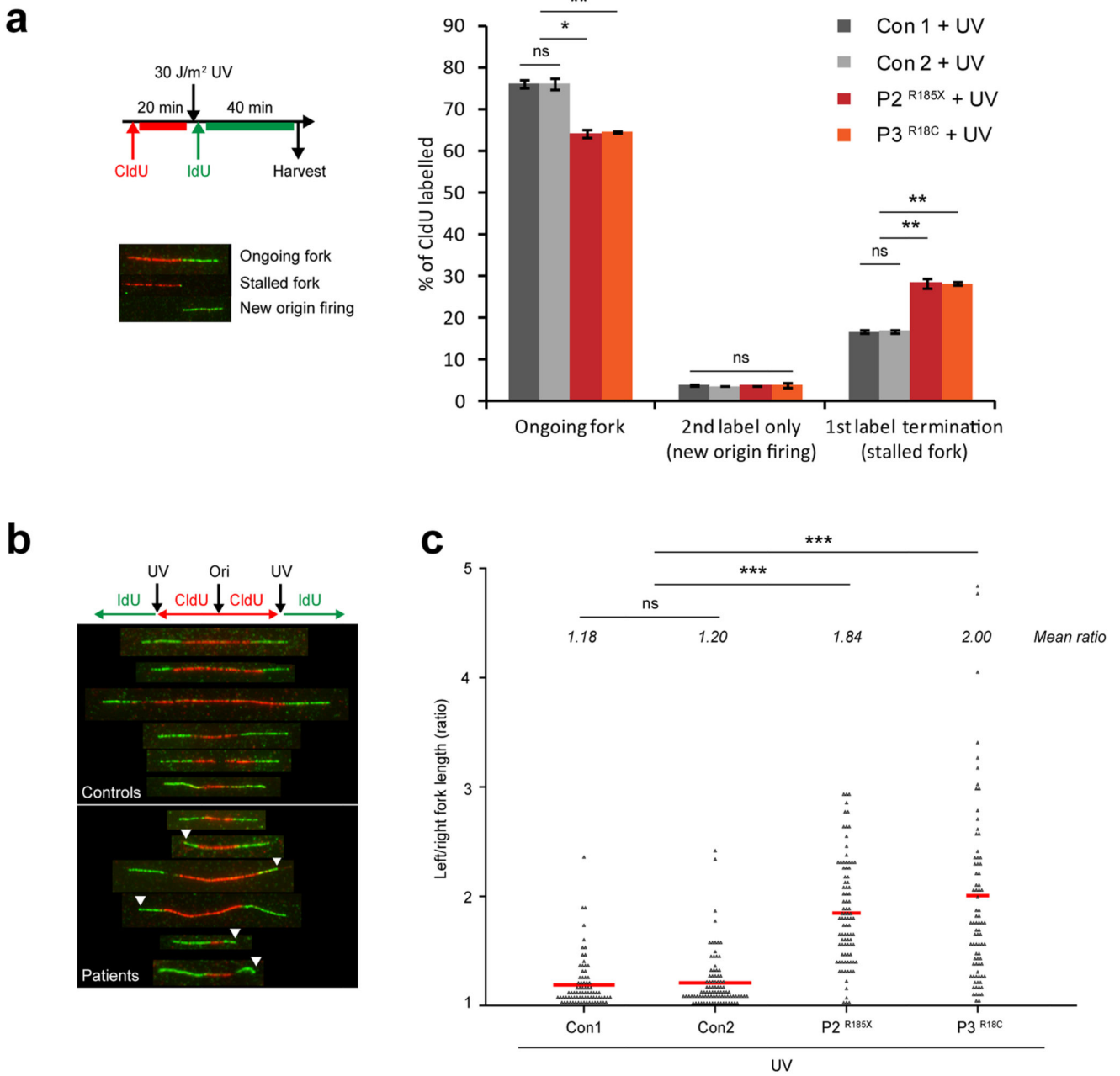
Figure 6. Replication fork stalling is increased following UV-induced DNA damage in TRAIP patient cells

(**a**) First label termination events (representing elevated replication fork stalling) are increased after UV irradiation in TRAIP patient fibroblasts. Top left panel, schematic of the experimental plan. Bottom left panel, representative images of ongoing or stalled replication forks and new origin firing from DNA fiber spreads of primary fibroblasts. Right panel, quantification of ongoing forks, 2nd label only (new origin firing) and 1st label termination (fork stalling) structures in fibroblast cells. Mean ± SD, n=3 independent experiments, >400 structures per cell line per experiment quantified. Student's *t*-test: *p<0.05; **p<0.01; ns,

not significant. (**b**, **c**) Substantial fork asymmetry is seen in UV-treated patient cells. (**b**) Representative images of DNA fibers from controls (Con1, Con2) and patient fibroblasts (P2, P3) after 30 J/m^2 UV treatment. (**c**) Quantification of replication fork asymmetry. Ratio of left/right fork length; mean ratio for each cell line is indicated in italics; Mann Whitney Rank sum test: ***p<0.001; ns, not significant. Data points pooled from n=2 independent experiments, >50 structures per cell line per experiment quantified.

Table 1

Clinical summary of individuals with *TRAIP* mutations

Individual	Gender	Consanguinity	Ancestry	Nucleotide mutation	Protein alteration	Gestation (weeks)	BWT (kg) *SD*	Age (years)	Height (cm) *SD*	OFC (cm) *SD*	Karyotype	Craniofacial features	Clinical synopsis
P1	F	NC	Italian	c.553C>T	p.Arg185*	37	1.95 *−2.7*	5	85.9 *−5.4*	44 *−6.5*	46, XX	Microcephaly, scaphocephaly, long narrow face, micrognathia.	IUGR; recurrent severe lower respiratory tract infections; delayed speech, 2 deceased siblings with similar phenotypes.
P2	M	NC	English	c.553C>T	p.Arg185*	32	1.2 *−2.2*	7	103.5 *−3.9*	40.7 *−8.3*	46, XY	Microcephaly, scaphocephaly, long narrow face, micrognathia.	IUGR; recurrent severe lower respiratory tract infections; moderate global developmental delay; hypertrichosis.
P3	M	3rd cousin	Turkish	c.52C>T	p.Arg18Cys	40	1.75 *−2.9*	3	80 *−4.6*	40.1 *−8.1*	46, XY	Microcephaly, long narrow face, micrognathia.	IUGR; asthma; mild global developmental delay.

All parents were demonstrated to be heterozygote carriers of the mutations identified, confirming appropriate segregation within the family. Age is shown in years at time of measurements. BWT, birth weight; SD, standard deviation from the population mean for age and sex; OFC, occipital frontal circumference; F, female; M, male; NC, non-consanguineous; IUGR, intrauterine growth restriction.